https://www.sciencedirect.com/science/article/abs/pii/S1010603017312753
DOI: 10.1016/j.jphotochem.2017.10.034

Influence of the *meso*-Substituent on Strongly Red Emitting Phenanthrene-fused Boron–dipyrromethene (BODIPY) Fluorophores with a Propeller-like Conformation

Ana B. Descalzo,[a,c] Hai-Jun Xu,[b,d] Zhen Shen,[b] Knut Rurack[a,*]

[a] Chemical and Optical Sensing Division, Bundesanstalt für Materialforschung und -prüfung (BAM), Richard-Willstätter-Str. 11, D-12489 Berlin, Germany.

[b] State Key Laboratory of Coordination Chemistry, School of Chemistry and Chemical Engineering, Nanjing University, Nanjing 210046, China

[c] present address: Dpmt. Organic Chemistry, Faculty of Chemistry, Complutense University of Madrid (UCM), Av. Complutense, s/n, 28040, Madrid (Spain)

[d] present address: College for Chemical Engineering, Jiangsu Key Laboratory for Biomass Based Green Fuels & Chemistry, Nanjing Forestry University, Nanjing 210037, Jiangsu, China

[*] E-mail: knut.rurack@bam.de

ABSTRACT Highly emissive phenanthrene-fused boron–dipyrromethene (PBDP) dyes have been spectroscopically characterized in a series of solvents. The influence of different substituents (–H, –I, –CN, –DMA or a 15C5-crown ether) in the *para*-position of a phenyl ring attached to the *meso*-position of the BODIPY core is discussed. This family of dyes has an intense emission at $\lambda \geq 630$ nm, with fluorescence quantum yields between 0.7 and 1.0 in all solvents studied, except in the case of the dimethylamino-substituted derivative, **PBDP-DMA**, which undergoes excited-state intramolecular charge transfer (CT), leading to broadband dual fluorescence in highly polar solvents. Introduction of a weaker electron donor such as a benzocrown to the *meso*-position is not able to trigger a second (charge or electron transfer) process and, interestingly, heavy atom (iodine, **PBDP-I** derivative) substitution at that moiety does also not have a relevant influence on the photophysics, i.e., enhanced intersystem crossing was not observed. Electrochemical studies of **PBDP-DMA** complement the data reported and stress the fact that the decrease in fluorescence of **PBDP-DMA** in highly polar solvents is due to an excited-state CT process rather than to a photoinduced electron transfer (PET).

https://www.sciencedirect.com/science/article/abs/pii/S1010603017312753
DOI: 10.1016/j.jphotochem.2017.10.034

KEYWORDS: BODIPY dyes, ring fusion, fluorescence, charge transfer

INTRODUCTION

4,4-Difluoro-4-bora-3a,4a-diaza-s-indacene (or as commonly known, BODIPY®) dyes, see basic structure of compound **1** in Scheme 1, are a very popular family of dyes due to their very strong fluorescence emission, high absorption coefficients, and versatile chemistry [1,2]. The last is especially remarkable since it allows the introduction of diverse chemical groups to the dipyrrin core at all available positions for different purposes. BODIPYs have been employed as fluorescent labels for the detection of biomolecules [3,4] or cell imaging [5,6]. They have also been used as photosensitizer agents in photodynamic therapy [7,8], as light harvesting components in dye-sensitized solar cells [9,10], and as active fluorophore components in molecular switches [11,12] or chemical probes [13]. Regarding fluorescent probes, some representative examples are shown in Scheme 1. In the case of compound **3** [14], aldehyde condensation in the 3-position allows the introduction of a *p*-(*N*,*N*-dimethylamino)styryl unit for its application as a near-infrared (NIR) pH probe. Examples of functionalization in the *p*-position of the *meso*-phenyl ring include compounds of **series 4**. The introduction of amino groups enables the development of pH or metal ion sensitive probes [15,16], or, if a –OH function is introduced, as in compound **5**, the dye can be employed as pH sensor for the basic interval [17]. Anion sensing is also possible, as shown by the thiourea derivative **6**, a fluoride sensor [18].

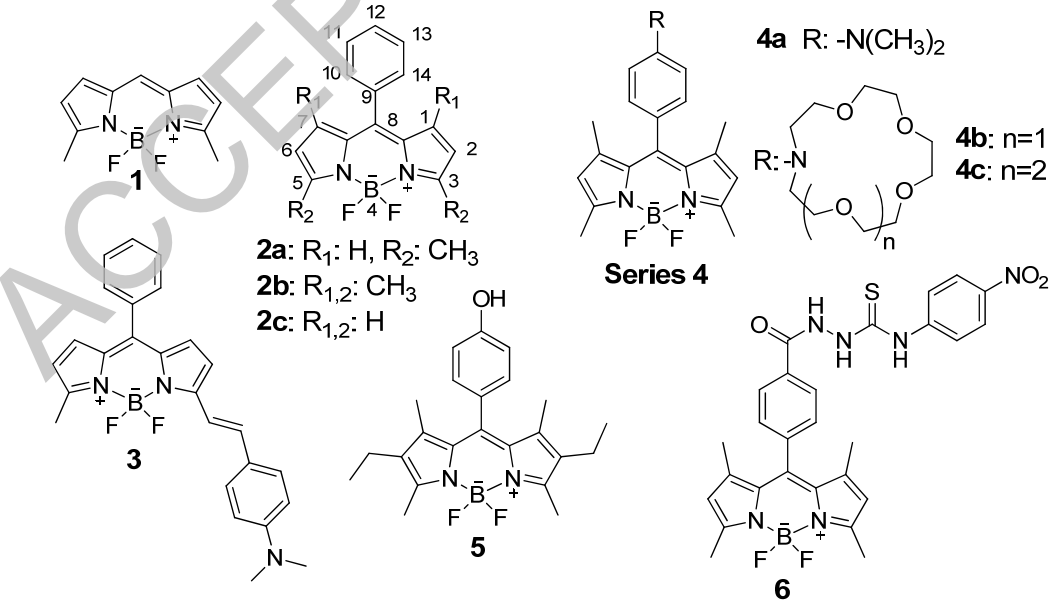

Scheme 1. Some literature examples of simple (**1**–**2**) and functional (**3**–**6**) BODIPY dyes. BODIPY derivatives in **series 4** have been employed as cation fluorescent probes: **4a** for H^+, **4b** for alkaline and

https://www.sciencedirect.com/science/article/abs/pii/S1010603017312753
DOI: 10.1016/j.jphotochem.2017.10.034

alkaline-earth metals [15] and **4c** for Pb^{2+} [16]. Moreover, while **3** [14] and **5** [17] respond to pH, **6** can be used for fluoride anion sensing [18].

Chemical modification of the simple BODIPY core **1** by condensation of additional π-conjugated units may additionally permit a decrease of the HOMO–LUMO band gap, resulting in bathochromic shifts of the absorption and emission bands [19,20]. The last is especially important when aiming to design fluorescent labels for low-background fluorescence-based analysis in biological systems [21,22]. However, it has to be taken into account that smaller HOMO–LUMO energy gaps tend to accelerate internal conversion (IC) processes [14]. A strategy for gaining a bathochromic shift of spectral bands while keeping the high emission efficiency of BODIPYs is direct fusion of rigid π-conjugated systems. The rigid structure is then less prone to undergo IC processes. Another factor that might decrease the emission efficiency in *meso*-phenyl substituted BODIPYs is rotation of the phenyl ring around the interannular bond, accelerating non-radiative processes, as it happens for example for compound **2a** (Φ_f = 0.19 in MeOH) [23] which has a lower quantum yield of fluorescence than its twin **2b** with additional methyl substituents in the 1 and 7 positions (Φ_f = 0.65 in MeOH) [15]. These methyl groups hinder free rotation of the *meso*-phenyl group. However, if the π system is extended by ring fusion to the BODIPY core, steric crowding may result which can force the chromophore and the appended subunit into conformations that are different from the classic planar dipyrrin system with orthogonally decoupled substituent in the *meso*-position. Hence, the *meso*-group can in principle come into resonance with the main chromophoric π system, potentially leading to novel spectroscopic behaviour.

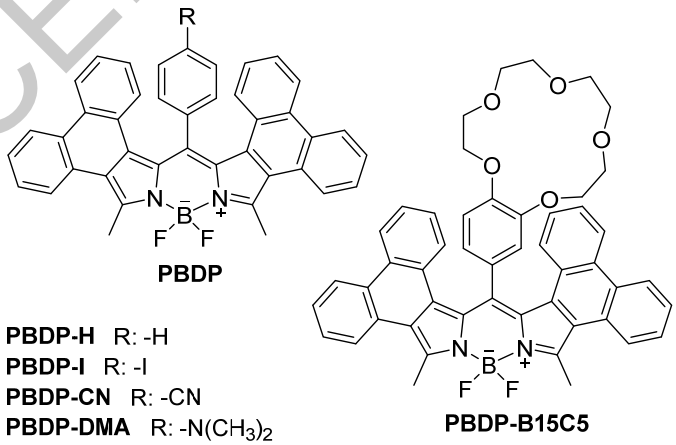

Scheme 2. Chemical structure of the phenanthrene-fused BODIPY dyes described in this work.

https://www.sciencedirect.com/science/article/abs/pii/S1010603017312753
DOI: 10.1016/j.jphotochem.2017.10.034

Here, we report a detailed investigation of phenanthrene-fused BODIPY dyes. Such dyes have been recently synthesized by us and used for chemical staining of polymer beads [24]. The strategy of phenanthrene fusion proved to be promising because positions which are normally employed for introducing chemical functions to the dye, such as the methyl groups at the 3- and 5- positions, or the positions of the *meso*-phenyl group, are still available. The family of dyes that are shown in Scheme 2 fulfill the above-mentioned conditions: i) π-extended rigid electronic structure via condensation of phenanthrene rings to the core; ii) dimethylamino, benzocrown ether or other substituents present in the *meso*-phenyl group; iii) availability of methyl groups in the 3- and 5- positions, and iv) sterically hindered rotation of the *meso*-phenyl substituent. In general, the title dyes were found to be highly emissive in the red/NIR region of the spectrum [24], yet a comprehensive spectroscopic characterization of this family of dyes was still missing.

EXPERIMENTAL

The compounds shown in Scheme 2 were prepared as described previously [24]. All the solvents employed for the spectroscopic measurements were of UV-spectroscopic grade and purchased from Aldrich.

Steady-state absorption and fluorescence measurements were carried out on a Cary 5000 UV/vis/NIR spectrophotometer and a Spectronics Instrument 8100 spectrofluorometer. For all measurements, the temperature was kept constant at 298 ± 1 K. Molar absorption coefficients were determined from $N = 4$ independent measurements and the uncertainties amount to ± 3100 M^{-1} cm^{-1}. For the fluorescence experiments, only dilute solutions with an absorbance of less than 0.1 at the absorption maximum were used. Fluorescence measurements were performed with a 90° standard geometry, with polarizers set at 54.7° for emission and 0° for excitation. Excitation at 580 nm was used for most experiments. The fluorescence quantum yields (Φ_f) were determined relative to rhodamine 101 in ethanol ($\Phi_f = 1.00 \pm 0.02$) [25] by using cresyl violet in methanol as a chemical transfer standard [1919,26]. All the fluorescence spectra presented here were spectrally corrected as described in [27]. The uncertainties of measurement were determined to ± 3 % (for $\Phi_f > 0.2$) and ± 6 % (for $0.2 > \Phi_f > 0.01$).

Fluorescence lifetimes (τ_f) were determined by a unique customized laser impulse fluorometer with picosecond time resolution which was described in earlier publications [28]. The fluorescence was collected at right angles (polarizer set at 54.7°; monochromator with

https://www.sciencedirect.com/science/article/abs/pii/S1010603017312753
DOI: 10.1016/j.jphotochem.2017.10.034

spectral bandwidths of 4, 8, and 16 nm) and the fluorescence decays were recorded with a modular single photon timing unit described in [28]. While realizing typical instrumental response functions of *fwhm* of ca. 25–30 ps, the time division was 4.8 ps channel^{-1} and the experimental accuracy amounted to ± 3 ps, respectively. The laser beam was attenuated using a double prism attenuator from LTB and typical excitation energies were in the nanowatt to microwatt range (average laser power). The fluorescence lifetime profiles were analyzed with a PC using the software package Global Unlimited V2.2 (Laboratory for Fluorescence Dynamics, University of Illinois). The goodness of the fit of the single decays as judged by reduced chi-squared (χ_R^2) and the autocorrelation function *C(j)* of the residuals was always below $\chi_R^2 < 1.2$. For all the dyes except **PBDP-DMA** in acetone, acetonitrile and methanol, decays were recorded at three different emission wavelengths over the BDP-type emission spectrum and analysed globally. For **PBDP-DMA** in the polar solvents, eight decays were analysed globally. Such a global analysis of decays recorded at different emission wavelengths implies that the decay times of the species are linked while the program varies the pre-exponential factors and lifetimes until the changes in the error surface (χ^2 surface) are minimal, that is, convergence is reached. The fitting results are judged for every single decay (local χ_R^2) and for all the decays (global χ_R^2), respectively. The errors for all the global analytical results presented here were below a global $\chi_R^2 = 1.2$.

Cyclic voltammetry was performed in CH_2Cl_2/0.1 M TBAP (tetra-*n*-butylammonium perchlorate) on a Zahner Imbex electrochemical working station utilizing a three-electrode configuration with a platinum disk as the working electrode, $Ag/AgNO_3$ as the quasi-reference electrode and a platinum wire as the counter electrode. Redox potentials were referenced internally against ferrocenium/ferrocene (Fc^+/Fc). CV measurements were performed under an inert atmosphere in the dark with a scan rate of 100 mV s^{-1} at room temperature.

RESULTS AND DISCUSSION

Absorption and fluorescence properties

The shape of the absorption spectra of all compounds shows the typical features of BODIPY dyes, i.e., narrow bands with full width at half maximum (*fwhm*) values that are very similar in all cases and tend to increase only slightly with the polarity of the solvent. For example, for **PBDP-H** in hexane, THF and MeCN the band width is 780, 820 and 900 cm^{-1}, respectively, and similar values (from 700 to 1000 cm^{-1}) were observed for all compounds in the different

https://www.sciencedirect.com/science/article/abs/pii/S1010603017312753
DOI: 10.1016/j.jphotochem.2017.10.034

solvents. Furthermore, the spectral band positions vary very little with the polarity of the solvent. In the case of **PDBP-H** for example the shift from the least polar hexane (λ_{abs} = 630 nm) to the most polar acetonitrile (λ_{abs} = 625 nm) amounts only to 5 nm. The influence of the *meso*-substituent is stronger, and it depends on its electron donating or accepting properties. Absorption maxima are bathochromically shifted with respect to **PBDP-H** when the substituent in the *para*-position of the phenyl ring is an electron acceptor group, such as –CN, or hypsochromically shifted in the case of the –DMA electron donor. This trend shows a good correlation with the corresponding values of the Hammett constant [24]. As an illustration, the absorption spectra of the different compounds in acetonitrile are collected in Figure 1. The absorption spectrum of the protonated **PBDP-DMA** derivative has also been included, showing the expected red shift in absorption from 617 to 633 nm upon decreasing the electron donor strength. Representative molar absorption coefficients were determined in acetonitrile, yielding values of *ca.* 10^5 M^{-1} cm^{-1} for all dyes ($\log\varepsilon_{625}$ = 5.07, **PBDP-H**; $\log\varepsilon_{628}$ = 4.99, **PBDPI**; $\log\varepsilon_{637}$ = 4.98, **PBDP-CN**; $\log\varepsilon_{617}$ = 5.06, **PBDP-DMA**; and $\log\varepsilon_{622}$ = 5.02, **PBDP-B15C5**). All relevant data are collected in Table 1.

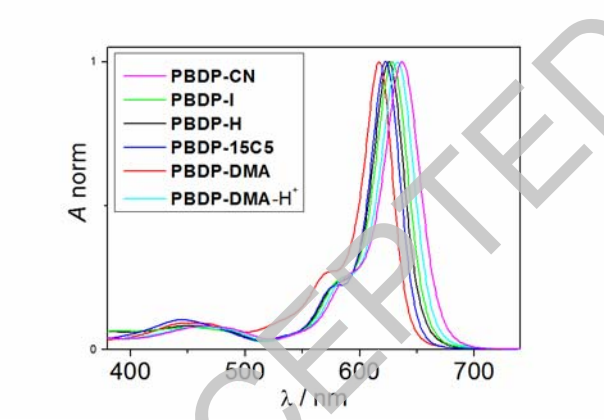

Figure 1. Normalized absorption spectra for compounds **PBDP-CN** (magenta), **PBDP-I** (green), **PBDP-H** (black), **PBDP-B15C5** (dark blue), **PBDP-DMA** (red) and protonated **PBDP-DMA** (cyan) in MeCN.

The emission is only a few nanometers red-shifted with respect to the absorption (300 cm^{-1} ≤ Stokes shift ≤ 700 cm^{-1} for all PBDPs in the series of solvents), as expected for BODIPY dyes. For all compounds, except for **PBDP-DMA** in highly polar solvents, the emission spectra are mirror images of the long-wavelength part of the absorption spectra and maxima are centered between 640 and 670 nm. The *fwhm* values oscillate between 800 and 1200 cm^{-1}, being generally *ca.* 100–150 cm^{-1} broader than those of the corresponding absorption spectra.

https://www.sciencedirect.com/science/article/abs/pii/S1010603017312753
DOI: 10.1016/j.jphotochem.2017.10.034

Table 1. Spectroscopic data of the PBDP dyes at 293 K.[a]

	solvent	λ_{abs} /nm	*fwhm* /cm^{-1}	λ_{em} /nm	*fwhm* /cm^{-1}	Φ_f	τ_f /ns	k_r^{obs} /10^8 s^{-1}	k_{nr}^{obs} /10^8 s^{-1}
PBDP-H	Hexane	630	780	647	920	0.94	5.92	1.6	0.1
PBDP-H	Bu_2O	630	770	648	920	1.01	5.75	1.7	0
PBDP-H	Et_2O	627	800	647	950	1.01	5.89	1.7	0
PBDP-H	THF	630	820	650	970	0.96	5.33	1.8	0.1
PBDP-H	Acetone	626	840	647	1000	0.97	5.87	1.7	0
PBDP-H	MeCN	625	900	647	1030	0.95	5.95	1.6	0.1
PBDP-H	MeOH	626	930	647	1050	0.81	5.74	1.4	0.3
PBDP-I	Hexane	633	800	652	950	0.98	5.64	1.7	0
PBDP-I	Bu_2O	633	820	654	970	0.92	5.65	1.6	0.1
PBDP-I	Et_2O	630	850	652	1010	0.92	5.98	1.5	0.1
PBDP-I	THF	633	880	656	1040	0.90	5.44	1.6	0.2
PBDP-I	Acetone	630	900	652	1070	0.89	5.91	1.5	0.2
PBDP-I	MeCN	628	930	652	1080	0.88	6.01	1.5	0.2
PBDP-I	MeOH	629	890	652	1050	0.76	5.67	1.3	0.4
PBDP-CN	Hexane	642	880	667	1030	0.90	6.03	1.5	0.2
PBDP-CN	Bu_2O	642	910	668	1060	0.95	5.92	1.6	0.1
PBDP-CN	Et_2O	639	910	666	1090	0.95	6.08	1.6	0.1
PBDP-CN	THF	642	930	670	1110	0.89	5.51	1.6	0.2
PBDP-CN	Acetone	638	960	667	1150	0.86	5.98	1.4	0.2
PBDP-CN	MeCN	637	1000	666	1170	0.80	5.98	1.3	0.3
PBDP-CN	MeOH	638	960	667	1160	0.73	5.31	1.4	0.5
PBDP-DMA	Hexane	621	690	634	830	1.02	5.77	1.8	0
PBDP-DMA	Bu_2O	621	710	636	840	0.96	5.54	1.7	0.1
PBDP-DMA	Et_2O	618	730	634	880	0.94	5.52	1.7	0.1
PBDP-DMA	THF	621	760	637	930	0.30	3.68	0.8	1.9
PBDP-DMA	Acetone	618	810	631, 771[b]	920, 3150[b]	0.033[c]	0.03 (85%)[d]	-[i]	-[i]
PBDP-DMA	MeCN	617	850	626, 798[b]	1090, 3200[b]	0.023[e]	0.02 (92%)[f]	-[i]	-[i]
PBDP-DMA	MeOH	617	880	629, 775[b]	1180, 4030[b]	0.060[g]	0.18 (73%)[h]	-[i]	-[i]
PBDP-B15C5	Hexane	626	730	640	860	0.96	5.61	1.7	0.1
PBDP-B15C5	Bu_2O	626	750	642	890	1.02	5.58	1.8	0
PBDP-B15C5	Et_2O	623	760	641	910	1.01	6.12	1.6	0
PBDP-B15C5	THF	626	780	644	930	0.98	5.68	1.7	0
PBDP-B15C5	Acetone	623	800	642	960	0.96	5.96	1.6	0.1
PBDP-B15C5	MeCN	623	850	643	960	0.96	5.16	1.6	0.1
PBDP-B15C5	MeOH	624	810	643	950	0.84	5.85	1.4	0.3

[a] $c_{dye} = 2 \times 10^{-6}$ M, λ_{exc} ~580 nm. [b] Maximum and half width of CT band. [c] Total Φ_f; 77 % CT contribution. [d] The decays are biexponential over the entire emission spectrum with a second decay time $\tau_f = 1.23$ ns. [e] Total Φ_f; 74 % CT contribution. [f] The decays are biexponential over the entire emission spectrum with a second decay time $\tau_f = 0.84$ ns. [g] Total Φ_f; 18 % CT contribution. [h] The decays are biexponential over the entire emission spectrum with a second decay time $\tau_f = 0.89$ ns. [i] See Table 2.

https://www.sciencedirect.com/science/article/abs/pii/S1010603017312753
DOI: 10.1016/j.jphotochem.2017.10.034

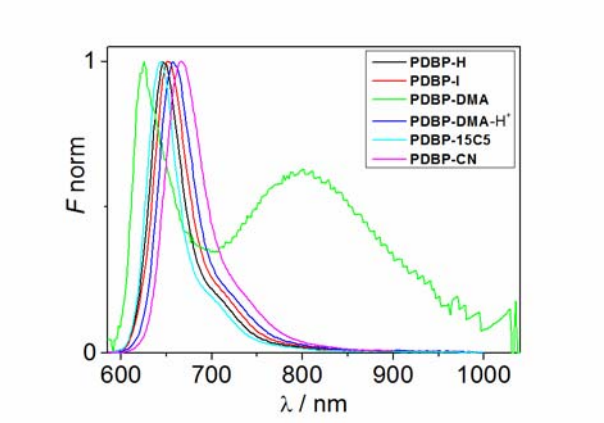

Figure 2. Normalized emission spectra for compounds **PBDP-H** (black), **PBDP-I** (red), **PBDP-DMA** (green), **PBDP-DMA**-H^+ (dark blue), **PBDP-B15C5** (cyan) and **PBDP-CN** (magenta) in MeCN.

The quenched fluorescence of **PBDP-DMA** in polar solvents is due to a fast CT process from the DMA donor group to the PBDP core, as reported for other *meso*-anilino-substituted BODIPYs [15,28,29]. The presence of this CT process generates dual emission and enables the fluorophore to be used as a NIR fluorescent probe that is "switched on" upon protonation (pK_a = 1.92) [24]. Partial protonation or solvation-mediated hydrogen bonding of the DMA group in the polar, protic solvent MeOH seems to partially inhibit the CT process, leading to a slightly higher quantum yield of fluorescence than in MeCN, a solvent of similar polarity (ε_T^{MeCN} = 35.94, $\Phi_f^{MeCN} = 0.023$; $\varepsilon_T^{MeOH} = 32.66$, $\Phi_f^{MeOH} = 0.060$; in the case of acetone: $\varepsilon_T^{Acetone} = 20.56$, $\Phi_f^{Acetone} = 0.033$). In Table 2, the ratio between the CT and LE bands (CT/LE entry) is shown.

The radiative rate constant k_r is very similar for all compounds in all solvents ($1.3 \times 10^{-8} \leq k_r \leq 1.8 \times 10^{-8}$ s^{-1}), except for **PBDP-DMA** in polar solvents: i) in THF $k_r^{PBDP\text{-}DMA}$ is 0.8×10^{-8} s^{-1}, while in the case of acetone, MeCN and MeOH, biexponential decays are obtained (Table 2). Assuming that the longest component should belong to the CT contribution, we have assessed the decay times for every species. Additionally, we have deconvoluted the steady-state emission bands and assigned every contribution to the Φ_f^{TOT} values, the overall fluorescence quantum yield, to two components: the locally excited (LE) state, corresponding to the band at shorter wavelengths in Figure 3 (Φ_f^{LE}), and the CT state, corresponding to the broader emission band at longer wavelengths (Φ_f^{CT}). On the basis of these values, an estimation of single k_r and k_{nr} has been made (Table 2). It is obvious that the rate of non-radiative processes that occur from the LE state are faster in the case of acetonitrile and acetone than in methanol, suggesting that hydrogen bonding between solvent and anilino-N is already effective in the ground state.

https://www.sciencedirect.com/science/article/abs/pii/S1010603017312753
DOI: 10.1016/j.jphotochem.2017.10.034

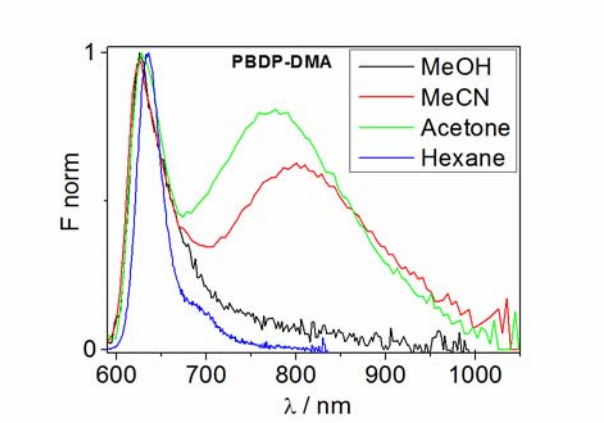

Figure 3. Normalized emission for **PBDP-DMA** in different solvents: MeOH (black), MeCN (red), acetone (green) and hexane (blue) (λ_{ex} = 580 nm).

Table 2. Spectroscopic data for **PBDP-DMA** dye at 293 K.[a]

Solvent	Φ_f^{Tot}	Φ_f^{LE}	Φ_f^{CT}	CT/LE	τ_f^{LE} /ns	τ_f^{CT} /ns	a_{rel}(LE)[b]	k_r^{LE} /10^8 s^{-1}	k_{nr}^{LE} /10^8 s^{-1}	k_r^{CT} /10^8 s^{-1}	k_{nr}^{CT} /10^8 s^{-1}
Acetone	0.033	0.0076	0.025	3.35	0.03	1.23	0.85	2.53	330.8	0.21	7.9
MeCN	0.023	0.0055	0.017	3.15	0.02	0.84	0.92	2.52	452.0	0.21	11.7
MeOH	0.060	0.049	0.011	0.22	0.18	0.89	0.73	2.81	54.3	0.12	11.1

[a] $c_{dye} = 2 \times 10^{-6}$ M, λ_{exc} ~580 nm. [b] Relative amplitude of the faster decay.

Besides the deactivation processes of the excited states involved, it is also important to assess their interplay. We thus invoked an analysis according to a formalism described in detail in [15]. The temporal evolution of a fluorescence decay corresponding to a two-state model as shown in Figure 4 can be described by a sum of two exponentials

$$I_{LE}(t) = A_{11}e^{-t(\tau_1)^{-1}} + A_{12}e^{-t(\tau_2)^{-1}} \quad (1)$$

$$I_{CT}(t) = A_{21}e^{-t(\tau_1)^{-1}} + A_{22}e^{-t(\tau_2)^{-1}} \quad (2)$$

with the two decay rates τ_i^{-1} directly observed in the experiment being linked to the species-related fluorescence lifetimes τ_0^X (X = LE, CT) through equations (3)–(6); A_{ij} are the corresponding amplitudes of the measured decay times τ_i at two different wavelengths in the regions of predominant LE and CT emission.

https://www.sciencedirect.com/science/article/abs/pii/S1010603017312753
DOI: 10.1016/j.jphotochem.2017.10.034

$$\frac{A_{12}}{A_{11}} = \frac{X - \tau_1^{-1}}{\tau_2^{-1} - X} \tag{3}$$

$$X = k_{LC} + (\tau_0^{LE})^{-1} \tag{4}$$

$$Y = k_{CL} + (\tau_0^{CT})^{-1} \tag{5}$$

$$\tau_{1,2}^{-1} = \frac{1}{2}\left\{(X+Y) \pm \left[(X-Y)^2 + 4k_{LC}k_{CL}\right]^{\frac{1}{2}}\right\} \tag{6}$$

Here, k_{LC} and k_{CL} are the rate constants of the excited state reactions and τ_0^{LE} is the lifetime of an unquenched model compound, e.g., **PBDP-H**. An analytical solution of eqs (3)–(6) yields the photophysical parameters given in Table 3. The rate constants of fluorescence deactivation of both emitting states can be compared when plotting the concentration ratio c_{CT} / c_{LE} as a function of time (s. eq. (7)) and calculating k_f^{CT} / k_f^{LE} from the ratio of both the fluorescence intensities and concentrations of the species (LE and CT) at equilibrium ($t \rightarrow \infty$) according to eq. (8). The latter, t_{eq}, is reached after ca. 0.1–0.2 ns.

$$\frac{c_{CT}(t)}{c_{LE}(t)} = \frac{k_{LC}(e^{-t(\tau_1)^{-1}} - e^{-t(\tau_2)^{-1}})}{(\tau_2^{-1} - X)e^{-t(\tau_1)^{-1}} + (X - \tau_1^{-1})e^{-t(\tau_2)^{-1}}} \tag{7}$$

$$\frac{\Phi_{CT}}{\Phi_{LE}} = \frac{k_f^{CT} c_{CT}(t)}{k_f^{LE} c_{LE}(t)} = \frac{k_f^{CT} k_{LC}}{k_f^{LE}[k_{LC} + (\tau_0^{CT})^{-1}]} \tag{8}$$

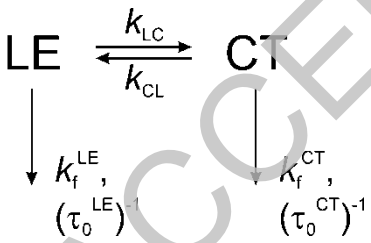

Figure 4. Generalized kinetic scheme for the photophysical processes that govern the excited state behavior of **PBDP-DMA**, involving two excited species (LE, CT).

Table 3. Calculated photophysical parameters of **PBDP-DMA** in acetone and MeCN at 298 K.[a]

solvent	A_{11}	A_{12}	k_{LC} /10^9 s^{-1}	k_{CL} /10^9 s^{-1}	$(\tau_0^{CT})^{-1}$ /10^9 s^{-1}	k_f^{CT} / k_f^{LE}	$t_{eq.}$ /ps
Acetone	15	85	28.3	4.8	0.92	0.57	180
MeCN	8	92	41.7	3.5	1.28	0.16	140

https://www.sciencedirect.com/science/article/abs/pii/S1010603017312753
DOI: 10.1016/j.jphotochem.2017.10.034

Compared with the 1,3,5,7-tetramethyl-substituted dipyrrin analogue **4a** (see Scheme 1), the CT process is distinctly slower (k_{LC} = 28 × 10^9 s^{-1} for **PBDP-DMA** in acetone [ε_r = 20.6] vs. 86 × 10^9 s^{-1} for **4a** in diethylether [ε_r = 4.2], see [15]). However, as seen for the dipyrrin analogue before, the ratios of k_f^{CT} / k_f^{LE} are <1 also in both solvents here, pointing to a forbidden nature of the CT state.

The brightness of the unquenched title dyes is exceptionally high, and distinctly higher than that of for instance the dipyrrin parent dyes **2b**,**c**, which is primarily due to Φ_f close to unity and logε ~ 5. Moreover, displaying τ_f of several nanoseconds, the much higher emissivity of for instance **PBDP-H** compared with **2b**,**c** is based on negligibly low non-radiative rate constants k_{nr}. Table 4 collects a relevant dataset for a better direct comparison of the annelated dyes with their parent chromophores.

Table 4. Photophysical parameters of **PBDP-H**, **2b** and **2c** in THF.[a]

	ε_{max} / M^{-1} cm^{-1}	Φ_f	$\varepsilon \times \Phi_f$ /M^{-1} cm^{-1}	τ_f / ns	k_r^{obs} /10^8 s^{-1}	k_{nr}^{obs} /10^8 s^{-1}	Ref.
PBDP-H	112,200	0.96	107,710	5.33	1.8	0.1	This work
2b	n.r.	0.25	n.c.	1.71	1.4	4.4	[30]
2c	60,000	0.023	1,380	0.26	0.9	37.6	[30]

[a] n.r. = not reported; n.c. = not calculated.

Redox properties

Cyclic voltammograms were measured for the PBDP dyes in CH_2Cl_2. The data are collected in Table 5 and a representative measurement is shown in Figure 4 for **PBDP-H**. In the case of **PBDP-DMA**, it is obvious that in the medium polar solvent the BDP core is oxidized before the dimethylanilino moiety, rendering electron transfer-type quenching unfavourable. Nonetheless, assessment of the driving force of a potential electron transfer (ET) quenching process is possible through the Rehm–Weller equation eq. (9):

$$\Delta G_{ET} = E(D^+/D) - E(A/A^-) - \Delta E_{00} - E_C \qquad (9)$$

Here, the free energy change ΔG_{ET} is related to the donor and acceptor ground-state potentials $E(D^+/D)$ and $E(A/A^-)$, respectively, the zero-zero transition energy ΔE_{00} of the chromophore, and the Coulomb stabilization energy of the formed radical ion pair in the respective solvent, E_C. ΔE_{00} is derived from (E_{abs}[max] + E_{em}[max])/2. For **PBDP-DMA** the values of λ_{abs} and λ_{em} in CH_2Cl_2 amount to 622 nm and 638 nm, respectively (with a Φ_f = 0.65). These values yield a ΔE_{00} of 1.97 eV. E_C is small though not negligible in medium polar solvents and was estimated

https://www.sciencedirect.com/science/article/abs/pii/S1010603017312753
DOI: 10.1016/j.jphotochem.2017.10.034

to 0.25 eV [31,32], assuming a charge separation distance of 6.5 Å between the centre of the 6-membered BDP ring and C_4 of the *meso*-phenyl ring. Combining these values with the redox data, an ET driving force ΔG_{ET} = +0.1 eV is calculated. In contrast to dipyrrin analogues such as **4a**, such an ET, or photoinduced electron transfer (PET), process is not significantly favoured in medium polar solvents for **PBDP-DMA**.

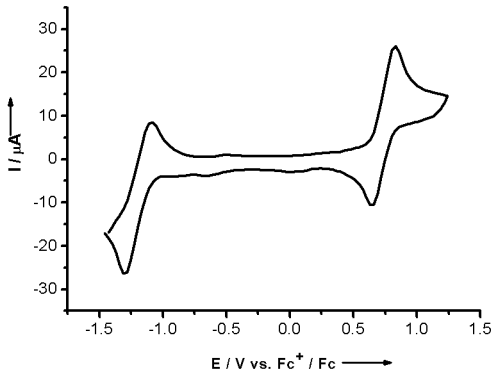

Figure 4. Cyclic voltammogram of **PBDP-H**, v = 100 mV s^{-1}, 0.1 M TBAP in CH_2Cl_2.

Table 5. Redox potentials of PBDP dyes (in CH_2Cl_2, c = 10^{-3} M, 0.1 M TBAP, v = 100 mV s^{-1}).

Compound	$E_{1/2}^{red}$ /mV	$E_{1/2}^{red}$ /mV	$E_{1/2}^{ox}$ /mV	$E_{1/2}^{ox}$ /mV
PBDP-H		–1200	720 (BDP)	
PBDP-I		–1170	830 (BDP)	
PBDP-CN	–1320 (PhCN)	–1050	870 (BDP)	
PBDP-DMA		–1300	780 (BDP)	1040[b] (DMA)

[a] Referenced against Fc^+/Fc. [b] Dimethylanilino moiety; assignment based on the fact that this wave vanishes in the presence of protons whereas the wave at 780 mV remains virtually unaltered.

Influence of molecular conformation and *meso*-substituent

As its short-wavelength absorbing and emitting counterpart **4a** [15], **PBDP-DMA** is also able to undergo CT state formation in the excited state and show dual fluorescence, yet the magnitude of the process is distinctly smaller, requiring highly polar solvents such as acetone or acetonitrile to invoke it. Furthermore, the propeller-like conformation of the dyes on one hand precludes too strong steric fixation in orthogonality that presumably hinders efficient CT state formation in dyes such as **8** (Scheme 3) [28]. The latter has also been observed for the parent dipyrrin dyes: sterically locked **11** lacks the red-shifted emission although its π system

https://www.sciencedirect.com/science/article/abs/pii/S1010603017312753
DOI: 10.1016/j.jphotochem.2017.10.034

is very similar to that of **4a**. On the other hand, the unique propeller-like orientation also suppresses CT absorption; like **9** which also exists in a propeller-like conformation [33], **PBDP-DMA** does also not show a broad and non-structured CT absorption band. This absorption band is found in compounds such as **10**, lacking substituents in the 1- and 7-positions of the BODIPY core [29]. The interannular twist angle θ, that lies between those of **9** and **10** for **PBDP-DMA** ($\theta_{\mathbf{10}} = 49°$, $\theta_{\mathbf{9}} = 60°$ and $\theta_{\mathbf{PBDP\text{-}DMA}} = 53°$), does not seem to be the only decisive parameter here, but steric crowding through π ring fusion has to be considered in addition. Compared with **9**, the CT process in **PDBP-DMA** is still weaker.

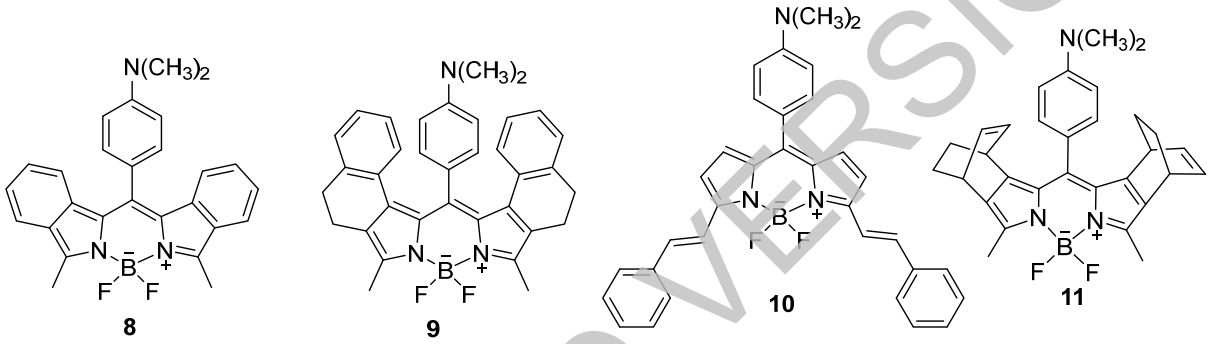

Scheme 3. *meso*-Electron donor-substituted dyes from the literature discussed in the text.

Quantum chemical calculations were carried out to better understand the photophysical behaviour of the dyes reported here. Optimization of the S_0 ground state geometries in the gas phase was performed with the density functional theory (DFT) method employing the hybrid functional B3LYP with a 6-31G basis set and energy-minimized as implemented in Gaussian 09 [34]. Figure 5 collects the frontier molecular orbitals of the three dyes **PBDP-H**, **PBDP-DMA** and **PBDP-CN**. Table 6 contains the calculated properties for the vertical excitation of the energy-minimized ground-state geometries [35].

Table 6 shows that for **PBDP-H** and **PDBP-CN** the lowest oscillator-strong transition is found at 546±10 nm in the gas phase, followed by a weaker transition at 485±8 nm and several distinctly weaker transitions up to ca. 400 nm (the next oscillator-strong transitions are only centred at < 300 nm). In case of **PBDP-DMA**, the lowest state (S_1) is less oscillator-strong and highly dipolar, involving HOMO–1 centred on the *meso*-aniline fragment and LUMO centred on the extended BODIPY fragment (Figure 5). The S_1 state is thus a CT state, which however is much more allowed than the respective states in the perpendicularly oriented parent

https://www.sciencedirect.com/science/article/abs/pii/S1010603017312753
DOI: 10.1016/j.jphotochem.2017.10.034

dyes such as **4a** and analogues [17]. In addition, it is much closer lying in energy to the BODIPY-centred, oscillator-strong S_2 state (ΔE_{S2-S1} = 0.01 eV), in contrast e.g. to **9** with ΔE_{S2-S1} = 0.22 eV, explaining why the CT process in **PBDP-DMA** needs even more polar solvents for activation than in **9**. Highly forbidden states are found for all three dyes at 428±15 nm, yet these are not CT states involving the *meso*-substituent, but transitions involving HOMO–3 (for **PBDP-H** and **PDBP-CN**) or HOMO–4 (for **PBDP-DMA**) which are exclusively centred on the appended phenanthrene units. Accordingly, this transition is not connected to a pronounced dipole moment change and thus not sufficiently stabilized even in highly polar media to unfold any quenching effect.

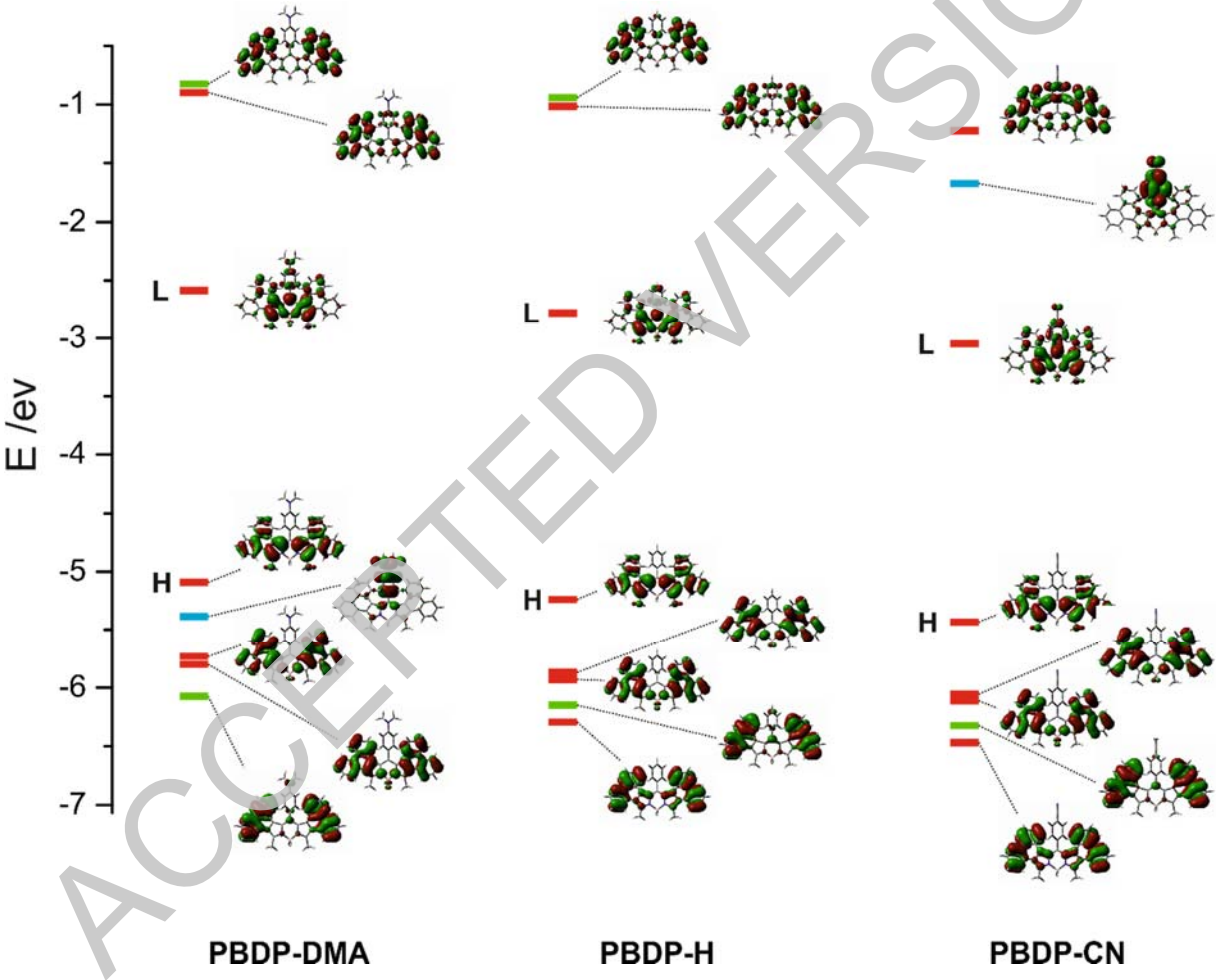

Figure 5. Frontier molecular orbitals of geometry-optimized **PBDP-H**, **PBDP-DMA** and **PBDP-CN**; HOMO and LUMO are denoted by "H" and "L", MOs localized on the entire phenanthro-BODIPY fragment in red, MOs localized on the *meso*-substituent in blue, MOs localized on (almost) exclusively the phenanthrene fragments in green.

https://www.sciencedirect.com/science/article/abs/pii/S1010603017312753
DOI: 10.1016/j.jphotochem.2017.10.034

Table 6. Calculated properties for the vertical excitation of the energy-minimized ground-state geometries of **PBDP-H**, **PBDP-DMA** and **PBDP-CN**.

	$\lambda_{S_n \leftarrow S_0}(n)$ /nm [a]	f [b]	$\Delta\mu_{S_n-S_0}$ /D [c]	Orbitals (coefficients) [d]
H	537.2 (1)	0.699	–2.1	HOMO–LUMO (0.69), HOMO–1–LUMO (–0.13)
	478.6 (2)	0.187	2.5	HOMO–LUMO (0.13), HOMO–1–LUMO (0.69)
	465.3 (3)	0.042	2.3	HOMO–2–LUMO (0.70)
	428.3 (4)	0.000	4.7	HOMO–3–LUMO (0.70)
	408.0 (5)	0.044	4.3	HOMO–4–LUMO (0.70)
DMA	532.3 (1)	0.091	**18.7**	HOMO–1–LUMO (0.71)
	529.9 (2)	0.710	–2.8	HOMO–LUMO (0.70), HOMO–2–LUMO (–0.11)
	469.0 (3)	0.155	1.9	HOMO–LUMO (0.11), HOMO–2–LUMO (0.69)
	451.8 (4)	0.078	1.7	HOMO–3–LUMO (0.69)
	412.2 (5)	0.007	4.2	HOMO–4–LUMO (0.69)
CN	555.0 (1)	0.631	3.5	HOMO–LUMO (0.69), HOMO–1–LUMO (0.14)
	494.5 (2)	0.174	0.6	HOMO–LUMO (–0.14), HOMO–1–LUMO (0.69)
	480.9 (3)	0.040	0.4	HOMO–2–LUMO (0.70)
	442.4 (4)	0.000	3.0	HOMO–3–LUMO (0.70)
	420.3 (5)	0.042	2.3	HOMO–4–LUMO (0.68)

[a] Wavelength of the transition. [b] Oscillator strength of the transition. [c] Dipole moment difference between ground (μ_0) and respective excited (μ_n) state. [d] MOs involved in the transitions.

Requiring already highly polar solvents to invoke the CT process in the derivative with the strongest electron donor in the present series, it is not surprising that **PBDP-B15C5** carrying the weaker electron donating benzocrown is not able to generate dual fluorescence. Also, *meso*-(*p*-cyanophenyl) substitution does not have any other effect than leading to the most bathochromically absorbing and emitting dye. The electron accepting group at the bridgehead carbon atom of the 6-membered dipyrrin ring best stabilizes the LUMO, which is well known to possess a sizeable orbital coefficient here (Figure 5). Moreover, although possessing significantly shifted HOMO and LUMO and a much smaller energy gap between them, *meso*-

https://www.sciencedirect.com/science/article/abs/pii/S1010603017312753
DOI: 10.1016/j.jphotochem.2017.10.034

4-iodophenyl substitution does also not influence the bright fluorescence significantly, like observed for green absorbing and emitting BODIPYs before [36].

In the literature, others and we have so far only been able to report on dual emissive BODIPY dyes that stretch across the wavelength range from the green to the red, i.e., commonly from 500–750 nm [15,23,37–39]. Here, we could extend this behavior to the NIR range, **PBDP-DMA** covering an impressive window from 600–950 nm while still showing reasonable fluorescence quantum yields of ca. 5%.

CONCLUSIONS

The detailed spectroscopic and electrochemical investigation of phenanthroline-appended BODIPY dyes has revealed interesting insight into the intramolecular charge-transfer behaviour of π-extended and thus sterically crowded boron–dipyrromethenes. A delicate interplay of structure and dual emission properties has been found, making it obvious how careful tuning of the BODIPY chromophore can yield powerful fluorescence dyes. While *meso*-4-cyanophenyl substitution leads to a dye that shows fluorescence quantum yields >0.8 in the 620–780 nm range in solvents of any polarity, *p*-iodo substitution at the *meso*-substituent is possible without influencing the fluorescence properties and *p*-(*N*,*N*-dimethylamino)phenyl substitution allows to obtain broadband emitters for the red/NIR spectral range. Further extension of the BODIPY's π system will tell in the future how much such fluorescence can be shifted into the range beyond 1000 nm.

ACKNOWLEDGEMENTS

ABD thanks the Spanish Ministry of Science and Innovation ("Ramón y Cajal" Program) and the Alexander von Humboldt Foundation for financial support.

https://www.sciencedirect.com/science/article/abs/pii/S1010603017312753
DOI: 10.1016/j.jphotochem.2017.10.034

REFERENCES

[1] A. Loudet, K. Burgess, BODIPY dyes and their derivatives: syntheses and spectroscopic properties, Chem. Rev. 107 (2007), 4891–4932.

[2] N. Boens, B. Verbelen, W. Dehaen, Postfunctionalization of the BODIPY core: synthesis and spectroscopy, Eur. J. Org. Chem. (2015) 6577–6595.

[3] D.Wang, J. Fan, X. Gao, B. Wang, S. Sun, X. Peng, Carboxyl BODIPY dyes from bicarboxylic anhydrides: one-pot preparation, spectral properties, photostability, and biolabeling, J. Org. Chem. 74 (2009) 7675–7683.

[4] S. Lim, M.M. Haque, D. Su, D. Kim, J.-S. Lee, Y.-T. Chang, Y.K. Kim, Development of a BODIPY-based fluorescent probe for imaging pathological tau aggregates in live cells, Chem. Commun. 53 (2017) 1607–1610.

[5] D.L. Marks, R. Bittman, R.E. Pagano, Use of BODIPY-labeled sphingolipid and cholesterol analogs to examine membrane microdomains in cells, Histochem. Cell Biol.130 (2008) 819–832.

[6] T. Kowada, H. Maeda, K. Kikuchi, BODIPY-based probes for the fluorescence imaging of biomolecules in living cells, Chem. Soc. Rev. 44 (2015) 4953–4972.

[7] S.G. Awuah, Y. You, Boron dipyrromethene (BODIPY)-based photosensitizers for photodynamic therapy, RSC Adv. 2 (2012) 11169–11183.

[8] A. Kamkaew, S.H. Lim, H.B. Lee, L.V. Kiew, L.Y. Chung, K. Burgess, BODIPY dyes in photodynamic therapy, Chem. Soc. Rev. 42 (2013) 77–88.

[9] S. Kolemen, O.A. Bozdemir, Y. Cakmak, G. Barin, S. Erten-Ela, M. Marszalek, J.-H. Yum, S.M. Zakeeruddin, M.K. Nazeeruddin, M. Grätzel, E.U. Akkaya, Optimization of distyryl-BODIPY chromophores for efficient panchromatic sensitization in dye sensitized solar cells, Chem. Sci. 2 (2011) 949–954.

[10] M. Mao, Q.-S. Li, X.-L. Zhang, G.-H. Wu, C.-G. Dai, Y. Ding, S.-Y. Dai, Q.-H. Song, Effects of donors of BODIPY dyes on the performance of dye-sensitized solar cells, Dyes Pigm. 141 (2017) 148–160.

[11] C. Trieflinger, K. Rurack, J. Daub, "Turn ON/OFF your LOV light": boron-dipyrromethene-flavin dyads as biomimetic switches derived from the LOV domain, Angew. Chem. Int. Ed. 44 (2005) 2288–2291.

https://www.sciencedirect.com/science/article/abs/pii/S1010603017312753
DOI: 10.1016/j.jphotochem.2017.10.034

[12] F. Puntoriero, F. Nastasi, T. Bura, R. Ziessel, S. Campagna, A. Giannetto, Molecular logics: a mixed BODIPY-bipyridine dye behaving as a concealable molecular switch, New J. Chem. 35 (2011) 948–952.

[13] N. Boens, V. Leen, W. Dehaen, Fluorescent indicators based on BODIPY, Chem. Soc. Rev. 41 (2012) 1130–1172.

[14] K. Rurack, M. Kollmannsberger, J. Daub, Molecular switching in the near infrared (NIR) with a functionalized boron-dipyrromethene dye, Angew. Chem. Int. Ed. 40 (2001) 385–387.

[15] M. Kollmannsberger, K. Rurack, U. Resch-Genger, J. Daub, Ultrafast charge transfer in amino-substituted boron dipyrromethene dyes and its inhibition by cation complexation: a new design concept for highly sensitive fluorescent probes, J. Phys. Chem. A 102 (1998) 10211–10220.

[16] H.W. Mbatia, D.P. Kennedy, C.E. Camire, C.D. Incarvito, S.C. Burdette, Buffering heavy metal ions with photoactive CrownCast cages, Eur. J. Inorg. Chem. (2010) 5069–5078.

[17] R. Gotor, P. Ashokkumar, M. Hecht, K. Keil, K. Rurack, Optical pH sensor covering the range from pH 0−14 compatible with mobile-device readout and based on a set of rationally designed indicator dyes, Anal. Chem. 89 (2017) 8437–8444.

[18] P. Ashokkumar, H. Weißhoff, W. Kraus, K. Rurack, Test-strip-based fluorometric detection of fluoride in aqueous media with a BODIPY-linked hydrogen-bonding receptor, Angew. Chem. Int. Ed. 53 (2014) 2225–229.

[19] Y.-H. Yu, A.B. Descalzo, Z. Shen, H. Röhr, Q. Liu, Y.-W. Wang, M. Spieles, Y.-Z. Li, K. Rurack, X.-Z. You, Mono- and di(dimethylamino)styryl-substituted borondipyrromethene and borondiindomethene dyes with intense near-infrared fluorescence, Chem. Asian. J. 1 (2006) 176–187.

[20] Y. Ni, W. Zeng, K.-W. Huang, J. Wu, Benzene-fused BODIPYs: synthesis and the impact of fusion mode, Chem. Commun. 49 (2013) 1217–1219.

[21] H. Kobayashi, M. Ogawa, R. Alford, P.L. Choyke, Y. Urano, New strategies for fluorescent probe design in medical diagnostic imaging, Chem. Rev. 110 (2010) 2620–2640.

[22] Z. Guo, S. Park, J. Yoon, I. Shin, Recent progress in the development of near-infrared fluorescent probes for bioimaging applications, Chem. Soc. Rev. 43 (2014) 16–29.

[23] W.W. Qin, M. Baruah, M. Van der Auweraer, F.C. De Schryver, N. Boens, Photophysical properties of borondipyrromethene analogues in solution, J. Phys. Chem. A 109 (2005) 7371–7384.

https://www.sciencedirect.com/science/article/abs/pii/S1010603017312753
DOI: 10.1016/j.jphotochem.2017.10.034

[24] A.B. Descalzo, H.-J. Xu, Z.-L Xue, K. Hoffmann, Z. Shen, M.G. Weller, X.-Z You, K. Rurack, Phenanthrene-fused boron-dipyrromethenes as bright long-wavelength fluorophores, Org. Lett. 10 (2008) 1581–1584.

[25] D.F. Eaton, Reference materials for fluorescence measurement, Pure Appl. Chem. 60 (1988) 1107–1114.

[26] K. Rurack, M. Spieles, Fluorescence quantum yields of a series of red and near-infrared dyes emitting at 600-1000 nm, Anal. Chem. 83 (2011) 1232–1242.

[27] U. Resch-Genger, D. Pfeifer, C. Monte, W. Pilz, A. Hoffmann, M. Spieles, K. Rurack, J. Hollandt, D. Taubert, B. Schönenberger, P. Nording, Traceability in fluorometry: Part II. Spectral fluorescence standards, J. Fluoresc. 15 (2005) 315–336.

[28] Z. Shen, H. Röhr, K. Rurack, H. Uno, M. Spieles, B. Schulz, G. Reck, N. Ono, Boron–diindomethene (BDI) dyes and their tetrahydrobicyclo precursors—en route to a new class of highly emissive fluorophores for the red spectral range Chem. Eur. J. 10 (2004) 4853–4871.

[29] K. Rurack, M. Kollmannsberger, J. Daub, A highly efficient sensor molecule emitting in the near infrared (NIR): 3,5-distyryl-8-(p-dimethylaminophenyl)-difluoroboradiaza-*s*-indacene, New J. Chem. 25 (2001) 289-292.

[30] J. Banuelos, A. Gomez-Infante, I. Valois-Escamilla, D. Cruz-Cruz, R. Prieto-Montero, I. Lopez-Arbeloa, T. Arbeloa and E. Peña-Cabrera, Synthesis, Properties, and Functionalization of Non-symmetric 8-MethylthioBODIPYs, Eur. J. Org. Chem. (2016) 5009–5023.

[31] G.J. Kavarnos, Fundamental concepts of photoinduced electron transfer, Top. Curr. Chem. 156 (1990) 21–58.

[32] A. Weller, Photoinduced electron transfer in solution: Exciplex and radical ion pair formation free enthalpies and their solvent dependence, Z. Phys. Chem., Neue Folge 133 (1982) 93–98.

[33] Y.-W. Wang, A. B. Descalzo, Z. Shen, X.-Z. You, K. Rurack, Dihydronaphthalene-fused boron–dipyrromethene (BODIPY) dyes: insight into the electronic and conformational tuning modes of BODIPY fluorophores, Chem. Eur. J. 16 (2010) 2887–2903.

[34] M.J. Frisch, et al., Gaussian 09 (Gaussian, Inc., Wallingford CT, 2009).

[35] Butterfly conformations as reported in [33] also converge for **PBDP-H**, **PBPD-DMA** and **PBDP-CN**. However, like for most of the series **9** dyes, they are energetically much less favoured than the propeller conformations (24, 37 and 38 kJ mol^{-1} for **PBPD-DMA**, **PBPD-CN** and **PBPD-H**). These conformations were thus not considered here any further.

https://www.sciencedirect.com/science/article/abs/pii/S1010603017312753
DOI: 10.1016/j.jphotochem.2017.10.034

[36] A. Burghart, H. Kim, M. B. Welch, L. H. Thoresen, J. Reibenspies, K. Burgess, 3,5-diaryl-4,4-difluoro-4-bora-3a,4a-diaza-*s*-indacene (BODIPY) dyes: Synthesis, spectroscopic, electrochemical, and structural properties, J. Org. Chem. 64 (1999) 7813–7819.

[37] R. Hu, E. Lager, A. Aguilar-Aguilar, J. Liu, J. W. Y. Lam, H. H. Y. Sung, I. D. Williams, Y. Zhong, K. S. Wong, E. Penaña-Cabrera, B. Z. Tang, Twisted intramolecular charge transfer and aggregation-induced emission of BODIPY derivatives, J. Phys. Chem. C 113 (2009) 15845–15853.

[38] H. Chong, E. Fron, Z. Liu, S. Boodts, J. Thomas, J. N. Harvey, J. Hofkens, W. Dehaen, M. Van der Auweraer, M. Smet, Acid-sensitive BODIPY dyes: synthesis through Pd-catalyzed direct C(sp^3)-H arylation and photophysics, Chem. Eur. J. 23 (2017) 4687–4699.

[39] K. Rurack, M. Kollmannsberger, U. Resch-Genger, J. Daub, A selective and sensitive fluoroionophore for Hg^{II}, Ag^{I}, and Cu^{II} with virtually decoupled fluorophore and receptor units, J. Am. Chem. Soc. 122 (2000) 968–969.